

# ELBO-T2IAlign: A Generic ELBO-Based Method for Calibrating Pixel-level Text-Image Alignment in Diffusion Models

Qin Zhou, Zhiyang Zhang, Jinglong Wang, Xiaobin Li, Jing Zhang\*, Member, IEEE,  
Qian Yu, Lu Sheng, Dong Xu, Fellow, IEEE,

**Abstract**—Diffusion models excel at image generation. Recent studies have shown that these models not only generate high-quality images but also encode text-image alignment information through attention maps or loss functions. This information is valuable for various downstream tasks, including segmentation, text-guided image editing, and compositional image generation. However, current methods heavily rely on the assumption of perfect text-image alignment in diffusion models, which is not the case. In this paper, we propose using zero-shot referring image segmentation as a proxy task to evaluate the pixel-level image and class-level text alignment of popular diffusion models. We conduct an in-depth analysis of pixel-text misalignment in diffusion models from the perspective of training data bias. We find that misalignment occurs in images with small sized, occluded, or rare object classes. Therefore, we propose ELBO-T2IAlign—a simple yet effective method to calibrate pixel-text alignment in diffusion models based on the evidence lower bound (ELBO) of likelihood. Our method is training-free and generic, eliminating the need to identify the specific cause of misalignment and works well across various diffusion model architectures. Extensive experiments on commonly used benchmark datasets on image segmentation and generation have verified the effectiveness of our proposed calibration approach.

**Index Terms**—Diffusion models, text-image alignment, evidence lower bound, referring image segmentation.

## I. INTRODUCTION

The rapid advancement of text-to-image (T2I) diffusion models has enabled them to generate unprecedented results from given texts. Recent studies have shown that text-conditional diffusion models not only can generate high-quality images but also encode text-image alignment information [1]–[3]. This information can be used for various downstream computer vision tasks, including image classification [4], [5], object detection [6], image segmentation [7], [8], and image editing [9]–[11]. For instance, some research reveals that attention maps in the denoising network encode object semantics [12], [13]. By effectively reusing these attention maps, diffusion models can be applied to semantic segmentation [12], and panoptic narrative grounding [14]. Other studies analyze the diffusion model’s loss function and utilize the loss value for image classification [4], [5]. Additionally, text-image alignment information can also be applied to text-guided image editing [9], [15] and compositional generation [16]–[18]. However, current methods could work well if diffusion model could achieve perfect text-image

Q. Zhou, Z. Zhang, J. Wang, X. Li, J. Zhang, Q. Yu, L. Sheng are with Beihang University, China (e-mail: zhoushui2023@buaa.edu.cn, 20377279@buaa.edu.cn, wjzy@buaa.edu.cn, zhang\_jing@buaa.edu.cn). D. Xu is with University of Hong Kong, China (e-mail: dongxu@hku.hk).

\*Corresponding author

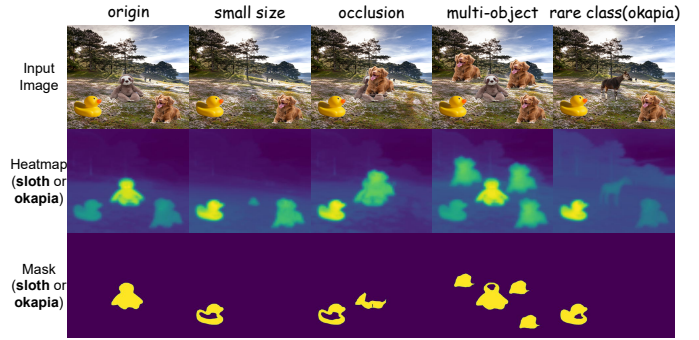


Fig. 1. Illustration of how different data issues affect pixel-text alignment of diffusion models using toy data. The poor alignment will lead to inaccurate semantic heatmaps and masks.

alignment, which is not the case. How to calibrate the text-image misalignment is the key to the downstream tasks that rely on precise text-image alignment.

In this paper, we examine the pixel-level image and class-level text alignment using zero-shot referring image segmentation as a proxy task, which can be effectively and quantitatively examined based on off-the-shelf semantic segmentation datasets. We find that one of the key reasons of the imperfect alignment between image pixels and textual classes stems from the highly biased dataset used for training the diffusion model. In the LAION dataset [19], images are crawled from the internet. However, these internet images are naturally long-tailed due to Zipf’s law of nature [20], which mostly contain only common object classes, not rare ones. And the long-tailed issue in LAION dataset has been validated by [21], [22]. Additionally, each image typically contains only a small number of classes. As a result, the text-image alignment is poorly established when multiple classes are present in a single image. We observe that when multiple classes appear in one image, the misalignment occurs with small sized, occluded, or rare object classes. Fig. 1 illustrates how different data issues affect pixel-text alignment in diffusion models using toy data (please see details in Section IV-A). The poor alignment will lead to inaccurate semantic heatmaps and masks.

To address these issues, we propose ELBO-T2IAlign, a simple yet effective training-free bias correction method to calibrate the pixel-text alignment. This generic approach works without needing to know the exact cause of misalignment, and works well across various diffusion model architectures. Specifically, we define an alignment score based on variational lower bound (ELBO) of the likelihood  $p_\theta(x|c)$ . Considering an image containing two object classes  $c_1$  and  $c_2$ , we claim

that  $c_1$  has stronger semantics if  $p_\theta(x|c_1) > p_\theta(x|c_2)$ . We find that diffusion models always focus on classes that have stronger semantics, leading to higher activation values in cross-attention maps. In an image with multiple classes, most classes will have low activation values in cross-attention maps. To obtain ELBO of the log-likelihood, we simply use the diffusion loss functions, which are proved to be written as functions of ELBO. Thus, we define the alignment score based on relative conditional diffusion loss values that encode information of ELBO of the log-likelihood. The alignment score corrects the cross-attention maps, ensuring that pixels of all object classes in an image have appropriate cross-attention activation values.

We conduct extensive experiments on 3 tasks: zero-shot referring image segmentation, image editing, and compositional generation. The results demonstrate that our ELBO-T2IAlign approach consistently improves pixel-text alignment across different diffusion model architectures.

The contributions of this paper are three-fold:

- We propose using zero-shot referring image segmentation as a proxy task to quantitatively evaluate the pixel-level image and class-level text alignment of popular diffusion models.
- We conduct an in-depth analysis of pixel-text misalignment in diffusion models from the perspective of training data bias.
- We propose ELBO-T2IAlign, a simple yet effective training-free generic method to correct pixel-text misalignment of diffusion models based on the ELBO of likelihood. Extensive experiments verified the effectiveness of our proposed correction approach on segmentation, image editing, and compositional generation.

## II. RELATED WORK

### A. Diffusion Models

Diffusion models have emerged as a new state-of-the-art (SOTA) in image and video generation, surpassing the Generative Adversarial Networks (GANs) [23]. These models generate samples by simulating a forward process that transforms data into noise and a reverse process that reconstructs data from noise. The foundational work, DDPM [24], established the framework for diffusion models, while DDIM [25] introduced a non-Markovian forward process that accelerates sampling. Latent Diffusion [26] integrates diffusion models with latent variables, improving computational efficiency. Classifier-Free Diffusion Guidance [27] provides a conditional classifier that directs models to generate specific categories. ControlNet [28] introduces control signals for precise image editing. Flow Matching [29], [30] uses optimal transport displacement interpolation to define the conditional probability paths, leading to better performance. Besides, research into diffusion models continues to explore new architectures, such as DiT [31], which uses Transformers instead of U-Net structures to enhance scalability and efficiency.

### B. Pixel-text Alignment Using Diffusion Models

With the exploration and utilization of the attention mechanisms in diffusion models, recent research has focused on

exploiting pixel-text alignment of the diffusion models through attention mechanism and applies the alignment nature to downstream tasks like semantic segmentation and image editing. For example, DiffSegmenter [12] extracts cross-attention maps and self-attention maps, and combines them to achieve zero-shot semantic segmentation. OVAM [32] and Diffu-Mask [3] utilize information from attentions to achieve pixel-level annotation of synthesized images. OVDiff [7] leverages generated data to extract prototype features, thereby utilizing the perception capabilities of diffusion models. DiffSeg [33] aggregates multi-layer self-attention maps to enable unsupervised segmentation with diffusion models. DiffPNG [34] uses the attention maps from diffusion as a basis, combined with the SAM [35] model, to generate detailed masks. InvSeg [34] utilizes attention information to extract anchor points, optimizing the latent space and enhancing segmentation accuracy. Differently, PTP [9], Shape-Guided Diffusion [36], CDS [37], and SAG [38] utilize attention maps for controllable image editing. However, these methods overlook the training data bias inherent in diffusion models, resulting in suboptimal performance in pixel-image alignment.

## III. METHOD

In this section, we first define our task setting, analyze the misalignment issues, and outline our motivations. We then present our ELBO-T2IAlign method in detail.

*a) Task definition:* Given an image  $x \in \mathbb{R}^{H \times W \times C}$  and candidate classes  $\{c_1, \dots, c_N\}$  in caption  $c$ , pixel-level image and class-level text alignment can be characterized by  $p_\theta(c_i|x_k)$ . Here,  $c_i$  indicates the  $i^{th}$  phrase that defines an object class,  $x_k$  represents the  $k^{th}$  pixel in image  $x$ , and  $N$  is the number of classes. In an ideal alignment, if the class label of pixel  $x_k$  is  $c_i$ , then  $p_\theta(c_i|x_k) > p_\theta(c_{j \neq i}|x_k)$ . We can generate segmentation masks directly using approximated  $p_\theta(c_i|x_k)$ . To examine the pixel-text alignment, we employ zero-shot referring image segmentation as a proxy task. Zero-shot RIS aims to segment reference objects  $c_i$  in image  $x$  based on image caption  $c$  without any training data, which can effectively reflect pixel-text alignment.

*b) Analyses of misalignment:* The misalignment between image pixels and textual classes could be caused by several reasons. We take two classes as an example. According to likelihood and Bayes' theorem, the posterior is,

$$p_\theta(c_1|x_k) = \frac{p(c_1)p_\theta(x_k|c_1)}{p(c_1)p_\theta(x_k|c_1) + p(c_2)p_\theta(x_k|c_2)}. \quad (1)$$

Suppose that the class label of  $x_k$  is  $c_1$ , an ideal alignment means  $p(c_1)p_\theta(x_k|c_1) > p(c_2)p_\theta(x_k|c_2)$ . However, misalignment happens in at least three cases in practice:

- 1)  $p(c_1) \ll p(c_2)$ , and  $p_\theta(x_k|c_1) > p_\theta(x_k|c_2)$
- 2)  $p(c_1) \approx p(c_2)$ , and  $p_\theta(x_k|c_1) < p_\theta(x_k|c_2)$
- 3)  $p(c_1) < p(c_2)$ , and  $p_\theta(x_k|c_1) < p_\theta(x_k|c_2)$

The first case stems from class imbalance with insufficient training data of  $c_1$  (e.g., rare object classes, or small objects presented in an image). The second case indicates that even different classes are approximately balanced, the wrong prediction could still happen due to class confusion between  $c_1$

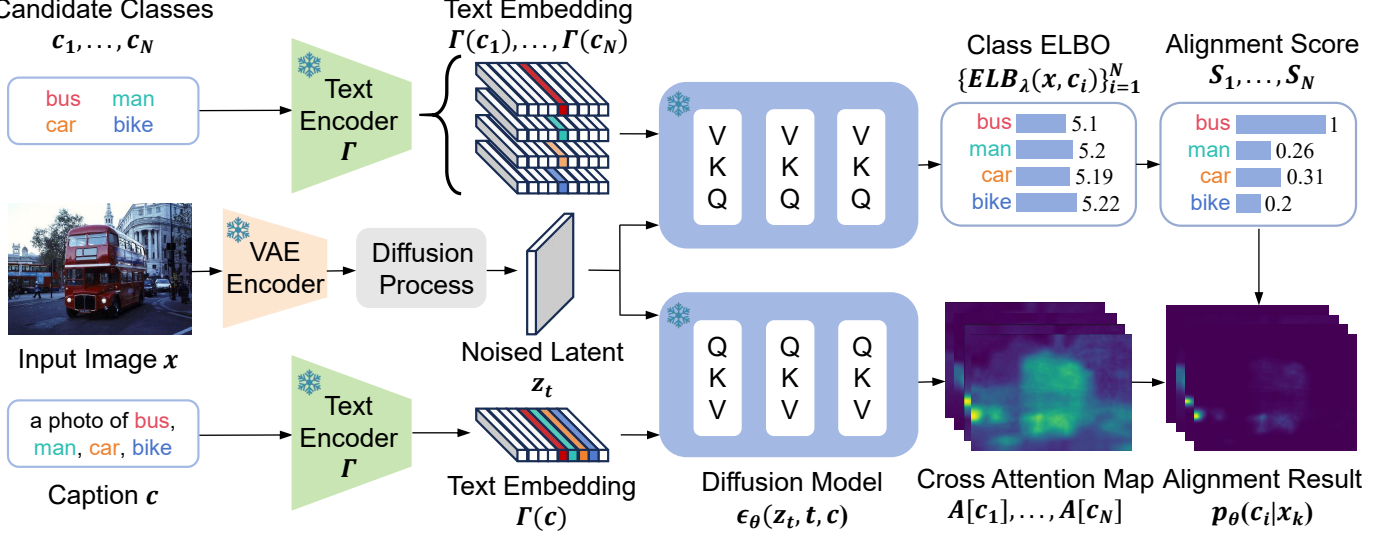


Fig. 2. **Pipeline of ELBO-T2IAlign.** Given a pre-trained frozen diffusion model, we approximate the rough pixel-text alignment through cross-attention map. Then, we compute the ELBO of likelihood  $p_\theta(x|c_i)$  of each class  $c_i$ . We define an alignment score based on ELBO, which is used for calibrate the cross-attention map. Segmentation masks are generated by applying threshold to  $p_\theta(c_i|x_k)$ .

and  $c_2$ , which can occur due to similar visual appearance between  $c_1$  and  $c_2$ , or when  $x$  is an out-of-training-distribution sample for class  $c_1$ . The third case combines both class imbalance and confusion.

*c) Motivation.* To correct the misalignment error, we propose modeling the semantic strengths present in an image using a variational lower bound (ELBO) of the log-likelihood  $p_\theta(x|c_i)$ , which is reflected by the diffusion loss function. We claim that  $c_1$  has stronger semantics if  $p_\theta(x|c_1) > p_\theta(x|c_2)$ . In this case, one class (e.g.,  $c_1$ ) will dominate the image, and the cross-attention maps of the other class (e.g.,  $c_2$ ) will have low activation values. We use ELBO of  $p_\theta(x|c_i)$  because it aligns closely with the training objectives of diffusion models. Moreover, the ELBO of  $p_\theta(x|c_i)$  can reflect the semantic strengths without needing to know the exact causes of misalignment.

*d) Preliminary of Conditional Diffusion Models.* Conditional diffusion model is a conditional generative model  $p_\theta(x|c)$  that approximates real conditional data distribution  $q(x|c)$ . In addition to the observed variable  $x$ , we have a series of latent variables  $z_t$  for timesteps  $t \in [0, 1]$ . Modern diffusion models process input in latent space. Condition encoder embeds condition  $c$  to embedding  $\Gamma(c) \in \mathbb{R}^{L \times D_c}$ . Encoder of specific autoregressive model maps observed  $x$  to latent  $x_0 \in \mathbb{R}^{H_z \times W_z \times D_z}$ . The model consists of a forward process and a reverse process. The forward process gradually adds noise to latent, which is a Gaussian diffusion process with marginal distribution  $q(z_t|x_0, c)$ :

$$z_t = \alpha_t x_0 + \sigma_t \epsilon \quad \text{where } t \in [0, 1], \epsilon \sim \mathcal{N}(0, I), \quad (2)$$

where  $\alpha_t$  and  $\sigma_t$  are function of  $t$ . The noise schedule (log signal-to-noise ratio) is given by  $\lambda(t) = 2\ln(\alpha_t/\sigma_t)$ .  $\lambda(t)$  is strictly monotonically decreasing, thus gradually transforming the origin  $x_0$  into pure Gaussian noise  $z_1$  in forward process. The reverse process is given by inverting the forward process using neural network  $\epsilon_\theta(z_t, t, c)$ .

*e) Overview.* An overview of our method is illustrated in Fig. 2. Given a pre-trained frozen diffusion model, we encode the input image  $x$  and caption  $c$  using visual and text encoders, respectively. The visual features undergo noising through the diffusion process. Subsequently, we feed the textual features and noised visual features into the pre-trained denoising model. We approximate the rough pixel-text alignment using the cross-attention map. Then, we compute the ELBO of likelihood  $p_\theta(x|c_i)$  for each class  $c_i$  by passing individual classes as conditions. Based on the ELBO, we define an alignment score, which we use to calibrate the posterior approximated by cross-attention maps.

#### A. Attention-Based Pixel-Text Alignment

In diffusion models, obtaining the exact  $p_\theta(c_i|x_k)$  is intractable. Previous methods approximate it either by the estimated likelihood [4], [5] or by using the cross-attention map [12], [13]. In this paper, we approximate the rough pixel-text alignment  $p_\theta(c_i|x_k)$  using the cross-attention map. Our method is applicable to all mainstream diffusion models since they all use attention mechanism [39] to condition  $x$  on  $c$  [9], [15], [18]. We collect cross-attention map  $A$  by one forward propagation of  $\epsilon_\theta(z_t, t, c)$ :

$$A = \text{softmax}\left(\frac{Q(z_t)K(c)^T}{\sqrt{d}}\right) \in \mathbb{R}^{(H_z \times W_z) \times L}, \quad (3)$$

where  $d$  is a scaling factor,  $Q(z_t), K(c)$  are visual query and textual key matrices respectively. Notice that (3) only represents one cross-attention layer. In practice, since diffusion models may have multiple cross-attention layers with different resolutions, we resize all cross-attention maps to the same resolution and average them to produce the final  $A$ . Interaction between modalities primarily happens in cross attention [26], [31], [40]–[42], which computes the similarity between visual query and textual key matrices. Higher cross-attention score

**Algorithm 1** Pixel-Text Alignment Calibration with ELBO

**Input:** Image  $x$ , caption  $c$ , candidate classes  $\{c_1, \dots, c_N\}$ , timestep  $t$  to collect attention maps

**Output:** Pixel-text alignment  $p_\theta(c_i|x_k)$  that can directly be processed to segmentation masks

- 1: Generate noised latent  $z_t$  based on (2)
- 2: Collect cross-attention map  $A$  based on (3)
- 3: Compute alignment score  $\{S_i\}_{i=1}^N$  based on (5)
- 4: **for**  $i = 1$  to  $N$  **do**
- 5: Extract corresponding columns of  $c_i$  in  $A$  and average them to obtain  $A[c_i] \in \mathbb{R}^{H_z \times W_z}$
- 6: Normalize:  $A[c_i] \leftarrow \text{min-max normalization}(A[c_i])$
- 7: Pixel-text alignment calibration:  $A[c_i] \leftarrow \sqrt[S_i]{A[c_i]}$
- 8: Class heatmap:  $H[c_i] \leftarrow \text{bilinear-upsample}(A[c_i])$
- 9: Enhance heatmap  $H[c_i]$  using self-attention map
- 10: **end for**
- 11: Stack all heatmaps and apply softmax to generate pixel-text alignment  $p_\theta(c_i|x_k)$  for  $\{c_1, \dots, c_N\}$

yields larger activation values in  $A$ , signifying a stronger relationship between the image pixel and the text label. Therefore, we can approximate  $p_\theta(c_i|x_k)$  by post-processing  $A$ . For each candidate class  $c_i$ , we first extract the corresponding columns in cross-attention map  $A$  and average these columns to obtain  $A[c_i] \in \mathbb{R}^{H_z \times W_z}$ . Then, we apply min-max normalization and bilinear upsample to  $A[c_i]$ , producing heatmap  $H[c_i] \in \mathbb{R}^{H \times W}$ . Next, we follow [12], [43] to further enhance the heatmap  $H[c_i]$  based on self-attention map that encodes correlations between different pixels. Finally, we generate pixel-text alignment  $p_\theta(c_i|x_k)$  using softmax. The algorithm is the same as Algorithm 1 without line 3 and line 7.

### B. Pixel-Text Alignment Calibration with ELBO

a) *Alignment Calibration with ELBO Objective*: Based on previous discussions on misalignment of  $x$  and  $c$ , we know pixel-text alignment  $p_\theta(c_i|x_k)$  from cross-attention is inaccurate. One straightforward method to improve the result is explicitly modeling pixel-text alignment, but this approach involves redesigning training objective and training from scratch, which is costly. We propose to leverage ELBO of  $p_\theta(x|c)$  from the pre-trained diffusion models to enhance  $p_\theta(c_i|x_k)$  prediction. The ELBO training objective of diffusion model is given by [44], [45]:

$$ELB_\lambda(x, c) = \frac{1}{2} \mathbb{E}_{t, \epsilon} \left[ -\frac{d\lambda}{dt} \|\epsilon_\theta(z_t, t, c) - \epsilon\|_2^2 \right], \quad (4)$$

where  $\lambda$  is the noise schedule given previously. As mentioned in the motivation of our method, if an image contains two object classes, we claim that  $c_1$  has stronger semantics if  $p_\theta(x|c_1) > p_\theta(x|c_2)$ . Therefore, the relative magnitude of ELBO training objective reflects the semantic strengths, and can be used as a signal to instruct the calibration of the attention maps as well as the corresponding approximated  $p_\theta(c_i|x_k)$ . We introduce an alignment score  $S = \{S_i\}_{i=1}^N$

TABLE I

$\omega(t)$  OF POPULAR DIFFUSION TRAINING OBJECTIVES. DIFFERENT OBJECTIVES LEVERAGE NEURAL NETWORK TO ESTIMATE DIFFERENT FUNCTIONS, AND USE LEARNED FUNCTION TO DO SAMPLING. SEE SECTION III-B AND SUPPLEMENTAL MATERIAL FOR MORE DETAILS AND DERIVATIONS.

Objective	Estimated Function	$\omega(t)$
Score [46]	$\nabla_{z_t} \ln q(z_t x)$	$-1/(\sigma_t^2 \cdot \lambda'(t))$
Flow [30]	$u(z_t \epsilon)$	$-(\sigma_t^2 \cdot \lambda'(t))/4$
X [48]	$x$	$-1/(\lambda'(t) \cdot e^{\lambda(t)})$
Epsilon [24]	$\epsilon$	$-1/\lambda'(t)$
Velocity [49]	$\alpha_t \epsilon - \sigma_t x$	$-(\alpha_t^2 + \sigma_t^2)^2/(\alpha_t^2 \cdot \lambda'(t))$

based on ELBO of  $p_\theta(x|c_i)$  to identify the semantic strengths of each class in image  $x$ :

$$S = \gamma^{\text{norm}(ELB_\lambda(x, c_1), \dots, ELB_\lambda(x, c_N))} \in \mathbb{R}^N, \quad (5)$$

where  $\gamma \in (0, 1]$  is a hyper-parameter. We transform ELBO objective into alignment score  $S_i \in [\gamma, 1]$  by applying simple min-max normalization and point-wise exponent. Intuitively, a higher alignment score  $S_i$  indicates  $c_i$  has a stronger semantic, and could better match with  $x$ . With the alignment score, we correct each  $A[c_i]$  by applying element-wise sqrt function with radical exponent  $S_i$ . This operation compensates for semantic loss during min-max normalization, thus getting better prediction of  $p_\theta(c_i|x_k)$ . The full algorithm is illustrated in Algorithm 1.

b) *Compute ELBO from Other Diffusion models*: Besides ELBO objective, recent diffusion models also use different objectives or mix objectives [24], [30], [46] instead of exact ELBO, which seems incompatible with our method. Fortunately, recent work [42], [47] showed all diffusion training objectives can be formulated as weighted ELBO. Despite different training objectives, we can still estimate the ELBO of  $p_\theta(x|c)$  by “unweighting” weighted ELBO objective if we assume  $\theta$  is well learned:

$$ELB_\lambda(x, c) \approx \frac{1}{2} \mathbb{E}_{t, \epsilon} \left[ \frac{1}{\omega(t)} \mathcal{L}_{\omega, \lambda}(x, t, c) \right], \quad (6)$$

where  $\mathcal{L}_{\omega, \lambda}(x, t, c)$  is the single timestep training objective of diffusion models. We list  $\omega(t)$  of popular training objectives in TABLE I, and give full derivation in supplementary. Furthermore, if we assume relative  $\|\epsilon_\theta(z_t, t, c_i) - \epsilon\|_2^2$  is stable among candidate classes in all timesteps, then relative relationship of alignment score will stay the same when using other objectives to replace  $ELB_\lambda(x, c_i)$ .

## IV. EXPERIMENTAL RESULTS

In this section, we evaluate pixel-text alignment through zero-shot referring image segmentation as a proxy task, and present results for compositional image generation and text-guided image editing.

### A. Pixel-text Alignment Results

a) *Datasets*: We evaluate our approach on the following five datasets. PASCAL VOC 2012 [50] contains 20 classes with 1,449 validation images. The PASCAL Context [51]

dataset includes 5,104 images for validation. We use the 59 most frequent classes, while the others are labeled as background. COCO 2017 [52] contains 5,000 images for validation. We use the 80 object classes and set other classes to background. Ade20K [53] contains 2000 images for validation across 150 object and stuff classes. To further verify our method on **Attribute-Enriched Prompts**, we synthesize a dataset named AEP. AEP contains 38 classes with attribute-enriched image captions (e.g. “three baby rabbits and a pink modern wooden suitcase”). We collect 741 captions from DVMP [18], generating and annotating images with FLUX [54] and Grounded SAM [55].

*b) Implementation Details:* For datasets that do not contain image captions, we concatenate all candidate classes  $\{c_i\}_{i=1}^N$  to produce the caption  $c$ . For example, if an image contains cat and hot dog, the image caption will be “a photo of cat, hot dog”. Each candidate class is a noun phrase in the caption, and we generate pixel-text alignment  $p_\theta(c_i|x_k)$  following Algorithm 1. To evaluate the result, we apply threshold to  $p_\theta(c_i|x_k)$ , generating background mask and labeling other pixels with the highest probability class. Then, we compare the mask produced by our method with ground truth. We mainly use mean Intersection over Union (mIoU) as the evaluation metric. We use FP16 as default data type to reduce memory usage and accelerate inference. We default sample 20 timesteps to compute ELBO and set  $\gamma = 1/3$ . More details can be found in supplementary.

*c) Baselines:* To verify the effectiveness of the pixel-text alignment enhancement by our method, we compare our method with the state-of-the-art diffusion-based segmentation methods, including DAAM [13], OVAM [32], DiffPNG [34], Semantic DiffSeg [33], and DiffSegmenter [12]. These methods can be easily adapted to our zero-shot referring image segmentation setting with few or no modifications. To ensure a fair comparison, the seed and text prompt are kept the same across different methods and other parameters are kept at their default values as provided. More details of baselines are in the supplemental material.

*d) Quantitative Comparisons with Baseline Methods:* TABLE II presents a quantitative comparison of zero-shot referring image segmentation results between our method and other state-of-the-art diffusion-based methods. We evaluate mIoU on four benchmark datasets. Compared to baseline methods, our approach shows significant improvements across different datasets, which demonstrates its strong alignment capability. Our method only performs poorer than DiffSegmenter [12] on the VOC dataset. We argue that since our method is designed to handle images that have multiple candidate classes, its effectiveness is less pronounced on the VOC dataset with fewer classes in an image.

*e) Qualitative Comparisons with Baseline Methods:* Fig. 3 illustrates the qualitative heatmap results comparing our method with other diffusion-based approaches. In the “monitor” case, the monitor appears at the edge of the image and is only partially visible. In the “sink” case, the sink occupies a very small portion of the image. In the “water” case, water is a background element that is not easily recognizable compared to other objects, making intentional localization challenging.

TABLE II  
RESULTS OF PIXEL-TEXT ALIGNMENT ON FOUR SEMANTIC SEGMENTATION BENCHMARK DATASETS.

Method	mIoU ↑			
	VOC	Context	COCO	Ade20K
DAAM [13]	48.11	26.13	29.16	15.02
OVAM [32]	47.45	25.17	25.72	11.68
DiffPNG [34]	53.18	35.49	28.98	18.59
DiffSegmenter [12]	<b>68.68</b>	39.47	38.88	22.88
Semantic DiffSeg [33]	44.34	24.29	20.34	9.80
ELBO-T2IAlign	<u>68.15</u>	<b>43.61</b>	<b>42.15</b>	<b>26.17</b>

In the “chair” case, the chair is obstructed by people and only the backrest is visible. The results indicate that our method achieves more precise localization and object contour capture for small objects like the sink, incomplete or obstructed objects like the monitor and chair, and less recognizable objects like water, compared to other methods. This demonstrates that our approach can better capture the semantic information of small or less prominent objects in multi-object scenes, reducing semantic confusion between different classes. We also present some segmentation masks generated by our method and other diffusion-based approaches in Fig. 4.

*f) Pixel-text Alignment Examination on Toy Data:* We conduct several toy experiments to examine how the semantic strength in an image affects the pixel-text alignment from pre-trained diffusion models. We observe at least four types of operations that reduce the semantic strength: small size, occlusion, multi-object, and rare class. Small size refers to proportionally scaling down an object, occlusion indicates occluding part of the object, multi-object refers to creating multiple copies of background objects, and rare class means replacing an object with a rarely seen object. We produce heatmaps and masks using Algorithm 1 without line 3 and line 7. As shown in Fig. 1, compared to the “origin” image, when reducing the size, or occlusion occurs, or multiple irrelevant objects present, the pixel-text alignment of the targeted sloth plushie is weakened. If we replace the target sloth plushie with a rare object (okapia), which has limited training data, the pixel-text alignment is also poor.

*g) ELBO-T2IAlign Results of Various Diffusion Models:* To demonstrate the generic nature of our method, we conduct experiments on diffusion models with different training objectives and architectures. The results are shown in TABLE III. It is evident that across all tested models whose training objectives are different, ELBO-T2IAlign consistently improves performance. This consistent improvement suggests that our refined strategy contributes significantly to the model alignment capability, regardless of the specific training objective and architecture of the model.

*h) ELBO-T2IAlign Results on Datasets with Attribute-enriched Prompts:* Since alignment score  $S$  is the core of our method, we conduct experiments on generating  $S$  with different candidate classes  $\{c_i\}_{i=1}^N$ . Specifically, we are interested in whether using whole noun phrase (e.g. “a red dog”) is better than single noun (e.g. “dog”) in (5). We show the results on our AEP dataset in TABLE IV. The results show that using

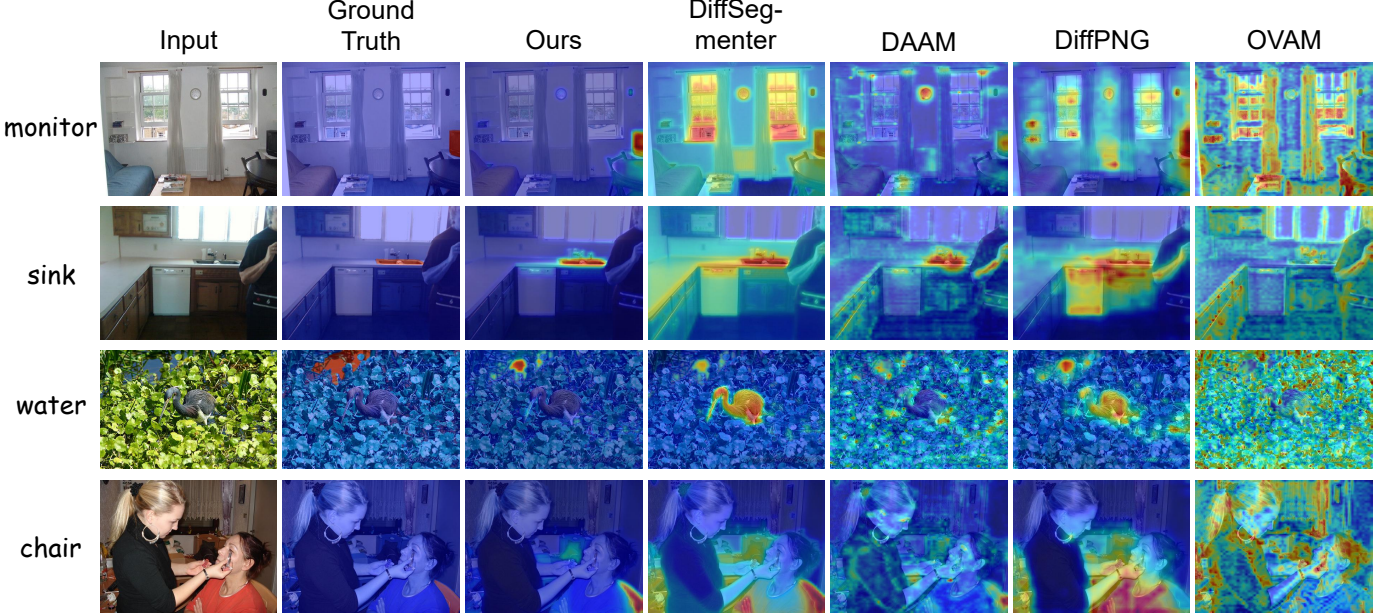


Fig. 3. **Pixel-text alignment heatmaps** generated by our proposed ELBO-T2IAlign and the state-of-the-art diffusion-based segmentation methods.

TABLE III

COMPARISON RESULTS OF **BEFORE** AND **AFTER** CALIBRATION USING OUR ELBO-T2IALIGN (ELB FOR SHORT) ACROSS VARIOUS DIFFUSION MODELS ON FOUR BENCHMARK DATASETS.

Model	ELB	mIoU $\uparrow$			
		VOC	Context	COCO	Ade20K
SD1.4		67.79	40.80	38.74	23.42
SD1.4	✓	<b>68.22</b>	<b>43.59</b>	<b>41.80</b>	<b>26.85</b>
SD1.5		67.57	40.61	39.19	22.66
SD1.5	✓	<b>68.15</b>	<b>43.61</b>	<b>42.15</b>	<b>26.17</b>
SD2		63.71	37.39	39.60	22.65
SD2	✓	<b>64.96</b>	<b>39.31</b>	<b>43.64</b>	<b>26.04</b>
SD2.1		67.6	40.70	41.37	23.41
SD2.1	✓	<b>69.04</b>	<b>42.41</b>	<b>44.53</b>	<b>26.32</b>
SDXL		57.72	33.28	34.89	17.87
SDXL	✓	<b>58.40</b>	<b>35.70</b>	<b>36.43</b>	<b>19.28</b>
SD3.5		51.17	36.23	35.25	22.54
SD3.5	✓	<b>51.74</b>	<b>37.27</b>	<b>37.31</b>	<b>25.01</b>

the whole noun phrase as a candidate class is better than using a single noun. Using more accurate candidate classes can lead to better results.

### B. Results on Image Generation and Editing

a) *Compositional Image Generation*: Our method can improve compositional generation using the proposed alignment score  $S$ . Given caption  $c$ , we extract entities and their visual attributes to obtain  $\{c_i\}_{i=1}^N$ . For each denoising step, we first estimate  $\epsilon$  using  $\epsilon_\theta(z_t, t, c)$ . Then, we follow (4) and (5) to estimate  $S$ . Finally, we use  $S$  for prompt reweighting [12], [56] to balance the semantics of  $\{c_i\}_{i=1}^N$  and estimate  $\epsilon$  with the reweighted prompt to denoise the latent. Specifically, when alignment score  $S_i$  is low, we increase the weight of class  $c_i$ . Balanced semantics allow the generated image to better

TABLE IV

COMPARISON RESULTS ACROSS VARIOUS DIFFUSION MODELS ON AEP DATASET. **ELB**: USE OUR ELBO-T2IALIGN FOR CALIBRATION. **AE**: USE ATTRIBUTE-ENRICHED NOUN PHRASE TO COMPUTE  $S$  IN (5).

Model	ELB	AE	mIoU $\uparrow$	Prec $\uparrow$	F1 Score $\uparrow$
SD1.5			58.70	68.77	72.62
SD1.5	✓		60.11	71.38	73.89
SD1.5	✓	✓	<b>60.58</b>	<b>71.66</b>	<b>74.18</b>
SDXL			52.55	64.29	67.53
SDXL	✓		53.81	66.33	<b>68.95</b>
SDXL	✓	✓	<b>53.82</b>	<b>66.96</b>	68.86
SD3.5			52.63	64.05	67.76
SD3.5	✓		52.46	<b>65.31</b>	67.77
SD3.5	✓	✓	<b>52.90</b>	65.13	<b>68.16</b>

represent extracted entities, thus improving text-image alignment. Following recent method [18], we evaluate our method on A&E [16], DVMP [18] and ABC-6K [17] datasets using CLIP score. We show results in TABLE V and visualize some images in Fig. 5. The results show that our ELBO-T2IAlign method consistently improves text-image alignment over the baselines. We provide full details and more experiment results in the supplementary.

b) *Text Guided Image Editing*: Various diffusion-based image editing methods are based on cross-attention manipulation. Our method can refine cross-attention maps thus improving image editing. Specifically, we use PTP [9] as baseline, which injects source text cross-attention to target text cross-attention to achieve editing. Given source text  $c$ , we extract entities and their visual attributes to obtain  $\{c_i\}_{i=1}^N$ . Then, we generate heatmaps of source text following Algorithm 1. Next, we scale these heatmaps based on source text cross-attention and use the scaled heatmaps to replace target text cross-attention. The visualization results are shown in Fig. 6.

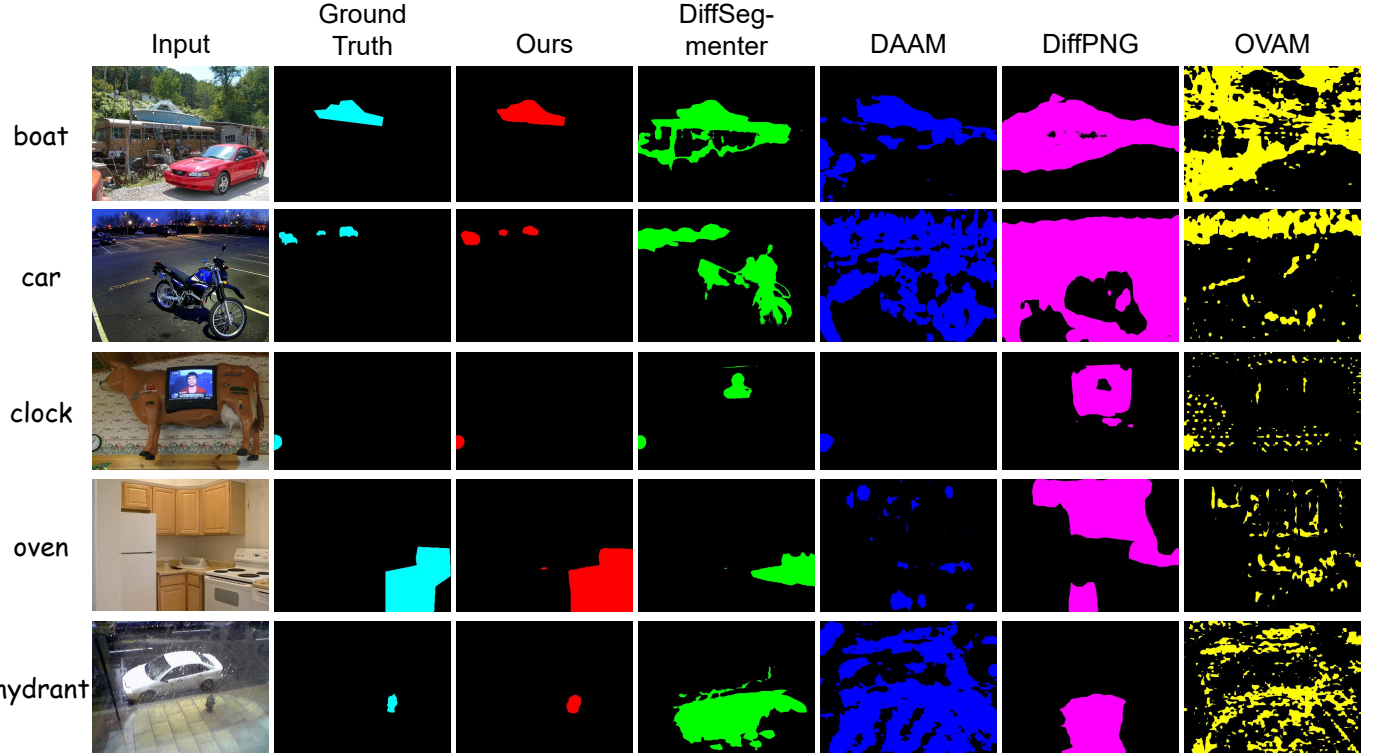


Fig. 4. **Segmentation masks** generated by our proposed ELBO-T2IAlign and the state-of-the-art diffusion-based segmentation methods.

TABLE V  
QUANTITATIVE COMPOSITIONAL IMAGE GENERATION RESULTS OF OUR  
ELBO-T2IALIGN AND THE BASELINES.

Method	Model	CLIP score ↑		
		A&E	DVMP	ABC-6K
Baseline	SD1.5	31.45	32.33	32.73
A&E [16]	SD1.5	<b>33.09</b>	32.24	32.48
SynGen [18]	SD1.5	31.83	32.18	32.45
ELBO-T2IAlign	SD1.5	<b>32.70</b>	<b>33.43</b>	<b>33.27</b>
Baseline	SD2.1	32.51	32.83	32.98
A&E [16]	SD2.1	<b>33.62</b>	33.16	32.86
SynGen [18]	SD2.1	32.20	32.34	32.70
ELBO-T2IAlign	SD2.1	<b>33.24</b>	<b>33.49</b>	<b>33.30</b>
Baseline	SDXL	33.61	34.27	33.22
ELBO-T2IAlign	SDXL	<b>33.72</b>	<b>34.45</b>	<b>33.37</b>

Our method can achieve editing more accurately with the scaled heatmaps. We give more results in the supplementary.

### C. Further Analyses

a) *Analysis of Computational Resources Cost*: We primarily employ Python 3.11.9, PyTorch 2.5.1, transformers 4.51.3 [57] and diffusers 0.33.1 [58] to implement our method on a single Ubuntu 20.04.3 LTS server with NVIDIA RTX 4090 graphics cards. Memory occupation of our method is very close to model’s forward propagation, because we only do forward propagation when computing ELBO and collecting attention maps. Our method uses approximately 7G memory for stable diffusion v1, v2 series, and uses approximately 13G

memory for stable diffusion XL series. For an image having 10 classes, our method takes around 4 seconds to generate all final masks on a single NVIDIA RTX 4090 graphics card with stable diffusion v1.5. If more GPU memory is available, our method can compute ELBO for all classes in a single batch to accelerate inference.

b) *Effect of Numbers of Timesteps to Compute ELBO*: To calculate ELBO objective, we sample timesteps evenly in the range  $[0, 1]$ . In TABLE VI we demonstrate the impact of numbers of sampling timesteps by varying the value of ELBO Timesteps  $\in \{1, 5, 20\}$  while keeping the other hyperparameters unchanged. Through observation, we find that with increasing number of sampling points, the mIoU on each dataset shows an upward trend. However, this increase is gradual, and the inference time rises with more sampling points. Therefore, we balance these factors and choose ELBO Timesteps = 20 as the default sampling step to calculate ELBO in our main experiment. We give more results in the supplementary.

c) *Effect of Sampling Strategy to Compute ELBO*: The definition of ELBO suggests that timesteps should be sampled uniformly for ELBO computation. We investigated whether alternative sampling strategies could yield better results. We present the results of different sampling strategies for ELBO computation in TABLE VII. For “Small”, “Middle” and “Large” strategies, we sample timesteps evenly from  $[0, 0.2]$ ,  $[0.4, 0.6]$  and  $[0.7, 0.9]$ , respectively. For “Random” strategy, we sample timesteps randomly from  $[0, 1]$ . For “Even” strategy, we sample timesteps evenly from  $[0, 1]$ . We use 10 timesteps for all sampling strategies to ensure fair comparison. The results align with our theoretical predictions. The “Ran-

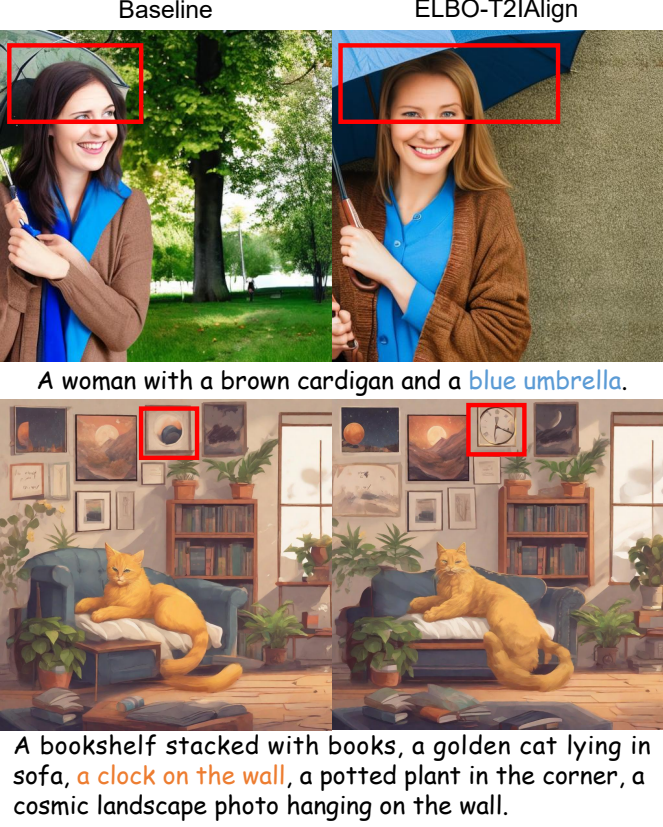


Fig. 5. Qualitative compositional generation results of **before and after** calibration using our ELBO-T2IAlign.

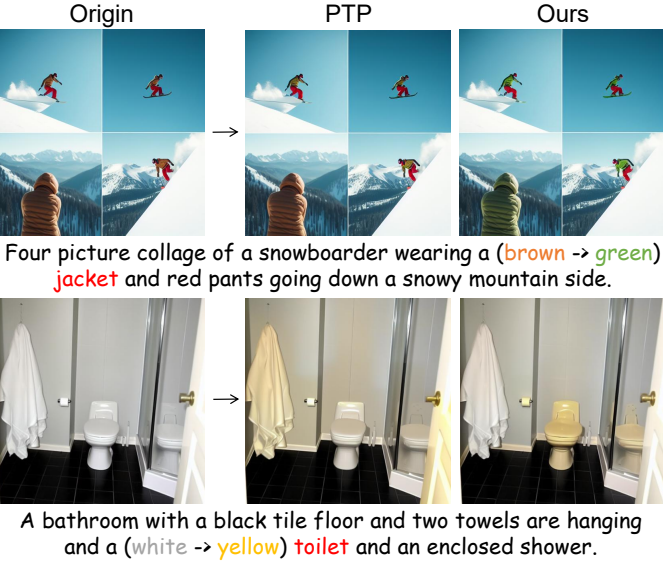


Fig. 6. Comparison results of image editing based on PTP [9] **before and after** calibration using our ELBO-T2IAlign.

dom” strategy is the best for computing alignment score and following by the “Even” strategy. Since these two strategies yield similar results, we adopt the “Even” strategy as default to reduce the randomness of our method. Comparing the results of “Small”, “Middle” and “Large” strategies reveals that larger timesteps experimentally improve ELBO computation, which

TABLE VI  
ELBO-T2IALIGN RESULTS ON FOUR BENCHMARK DATASETS WHEN USING DIFFERENT NUMBERS OF Timesteps TO COMPUTE ELBO.

Method	Steps	mIoU $\uparrow$			
		VOC	Context	COCO	Ade20K
SD1.5	1	67.35	40.58	39.80	24.58
SD1.5	5	68.15	42.28	41.36	24.93
SD1.5	20	<b>68.15</b>	<b>43.61</b>	<b>42.15</b>	<b>26.17</b>
SD2	1	63.00	35.63	40.32	23.57
SD2	5	63.50	38.21	42.57	24.65
SD2	20	<b>64.96</b>	<b>39.31</b>	<b>43.64</b>	<b>26.04</b>
SDXL	1	56.58	33.05	34.75	17.94
SDXL	5	58.14	34.43	36.01	18.73
SDXL	20	<b>58.40</b>	<b>35.70</b>	<b>36.43</b>	<b>19.28</b>

TABLE VII  
ELBO-T2IALIGN RESULTS ON FOUR BENCHMARK DATASETS WHEN USING ELBO Timesteps = 10 WITH DIFFERENT SAMPLING STRATEGY TO COMPUTE ELBO.

Model	Strategy	mIoU $\uparrow$			
		VOC	Context	COCO	Ade20K
SD1.5	Small	67.07	40.93	39.55	23.27
SD1.5	Middle	68.16	42.68	41.34	25.84
SD1.5	Large	<b>68.80</b>	42.97	41.46	25.79
SD1.5	Random	68.34	<b>43.21</b>	<b>41.86</b>	<b>26.15</b>
SD1.5	Even	68.18	<u>43.21</u>	<u>41.62</u>	<u>26.08</u>

may be related to the noise schedule  $\lambda(t)$ .

*d) Evaluations of Different  $\gamma$ :* In our method,  $\gamma$  in (5) is a critical hyperparameter that directly affects the ability of the ELBO to calibrate pixel-text alignment. An inappropriate value of  $\gamma$  can even worsen pixel-text alignment. Therefore, we varied  $\gamma^{-1} \in \{1, 2, 3, 4, 5, 6, 7, 8\}$  to observe its impact on mIoU. Our results show that the performance generally improves as  $\gamma$  decreases from 1 to around 1/2 or 1/3, but further decreases in  $\gamma$  tend to either plateau or result in a slight decline. This suggests that  $\gamma = 1/2$  or  $\gamma = 1/3$  will be the best choice. In our main experiment, we choose  $\gamma = 1/3$  as the default value. We show the pixel-text alignment results on four benchmark datasets in Fig. 7. To demonstrate that the effect is not due to the sqrt function itself, we fix alignment score  $\{S_i\}_{i=1}^N$  on line 7 of Algorithm 1. We set alignment score of each class to the same constant. As TABLE VIII shows, the results are better when ELBO is in effect.

*e) Effect of Different Attention Collecting Timesteps:* For simplicity, we only select one timestep  $t$  in Algorithm 1 to demonstrate our calibration process. In practice, we select multiple timesteps to generate pixel-text alignment results and average them. Different timesteps represent different stages in the diffusion process, with each timestep value affecting the data generated during inference. Both cross-attention and self-attention maps—which are fundamental to obtaining the final mask—are significantly influenced by timesteps, which in turn affect pixel-text alignment. To examine how timesteps influence pixel-text alignment during mask generation, we experiment with different timestep values while maintaining all other hyperparameters constant. To obtain attention maps,

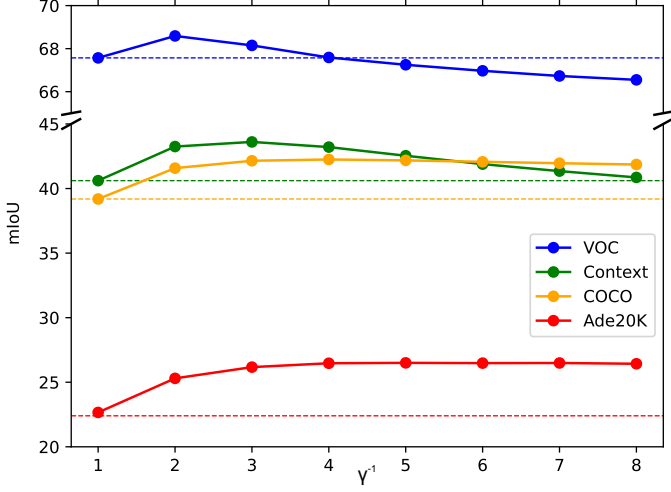


Fig. 7. How  $\gamma$  in (5) affects the segmentation results using Algorithm 1. The dotted lines indicate  $\gamma = 1$ , which means ELBO calibration is inactive.

TABLE VIII  
ELBO-T2IALIGN RESULTS ON FOUR BENCHMARK DATASETS WHEN ALIGNMENT SCORE  $S$  IS FIXED TO CONSTANT. THE RESULTS ARE BETTER WHEN ELBO IS IN EFFECT.

Method	Alignment Score $S$	mIoU $\uparrow$			
		VOC	Context	COCO	Ade20K
SD1.5	$S = 1/2$	66.61	40.29	40.13	22.90
SD1.5	$S = 1/3$	65.11	39.72	40.09	23.04
SD1.5	$S = 1/4$	63.28	38.69	39.58	22.87
SD1.5	ELB based $S$	<b>68.15</b>	<b>43.61</b>	<b>42.15</b>	<b>26.17</b>
SD2	$S = 1/2$	61.09	35.50	39.43	21.83
SD2	$S = 1/3$	58.45	33.22	38.97	21.24
SD2	$S = 1/4$	55.64	31.09	38.32	20.38
SD2	ELB based $S$	<b>64.96</b>	<b>39.31</b>	<b>43.64</b>	<b>26.04</b>
SDXL	$S = 1/2$	57.21	33.05	35.70	18.30
SDXL	$S = 1/3$	55.99	32.78	35.82	18.55
SDXL	$S = 1/4$	54.39	32.49	35.58	18.75
SDXL	ELB based $S$	<b>58.40</b>	<b>35.70</b>	<b>36.43</b>	<b>19.28</b>

we sample timesteps evenly within specific ranges. The parameter “Steps” in Table IX indicates the number of sampling timesteps and the “Strategy” defines the specific sampling range: “Small” corresponds to  $[0, 0.2]$ , “Middle” corresponds to  $[0.4, 0.6]$ , “Large” corresponds to  $[0.7, 0.9]$ , and “Random” means random sample from the range  $[0, 1]$ . Table IX demonstrates that the sampling range of timesteps significantly affects pixel-text alignment. Larger timesteps introduce more noise, which disrupts the original image information and leads to poorer alignment performance. Based on these findings, we set Steps=10 and use the range  $[0, 0.2]$  as our default values in the main experiment.

## V. CONCLUSIONS

Our research introduces a novel training-free and generic approach called ELBO-T2IALign, which leverages the evidence lower bound (ELBO) of likelihood to correct pixel-text misalignment in pre-trained diffusion models. We evaluated the alignment capabilities of popular diffusion models and uncovered the training data biases that lead to misalignment, particularly in images with small, occluded, or rare class

TABLE IX  
ELBO-T2IALIGN RESULTS ON FOUR BENCHMARK DATASETS WITH DIFFERENT ATTENTION COLLECTING STEPS AND STRATEGIES.

Model	Steps	Strategy	mIoU $\uparrow$			
			VOC	Context	COCO	
SD1.5	1	Small	67.97	42.38	41.41	25.92
SD1.5	10	Small	<b>68.18</b>	<b>43.21</b>	<b>41.62</b>	<b>26.08</b>
SD1.5	10	Middle	57.77	40.61	30.78	22.42
SD1.5	10	Large	37.69	27.47	18.72	14.27
SD1.5	10	Random	51.95	35.95	27.17	19.62
SD2	1	Small	62.52	39.56	37.37	23.27
SD2	10	Small	<b>64.62</b>	39.06	<b>43.09</b>	<b>25.43</b>
SD2	10	Middle	63.50	<b>40.29</b>	37.38	23.51
SD2	10	Large	44.25	31.32	23.43	16.89
SD2	10	Random	56.49	37.65	32.13	21.94

objects. Our proposed method offers an effective alignment calibration solution that is agnostic to the underlying cause of misalignment and compatible with diverse diffusion model architectures. The results are verified by extensive experiments. This work paves the way for more effective downstream tasks in image segmentation, image editing, and controllable generation. A limitation of this work is its reliance on the accuracy of the estimated ELBO of likelihood by pre-trained diffusion models. Nevertheless, despite this imperfect estimation, our method consistently improves performance.

## REFERENCES

- [1] Q. H. Nguyen, T. Vu, A. Tran, and K. Nguyen, “Dataset diffusion: Diffusion-based synthetic dataset generation for pixel-level semantic segmentation,” in *Thirty-Seventh Conference on Neural Information Processing Systems*, 2023.
- [2] W. Wu, Y. Zhao, H. Chen, Y. Gu, R. Zhao, Y. He, H. Zhou, M. Z. Shou, and C. Shen, “Datasetdm: Synthesizing data with perception annotations using diffusion models,” *Advances in Neural Information Processing Systems*, vol. 36, pp. 54 683–54 695, 2023.
- [3] W. Wu, Y. Zhao, M. Z. Shou, H. Zhou, and C. Shen, “DiffuMask: Synthesizing images with pixel-level annotations for semantic segmentation using diffusion models,” in *Proceedings of the IEEE/CVF International Conference on Computer Vision*, pp. 1206–1217. [Online]. Available: [https://openaccess.thecvf.com/content/ICCV2023/html/Wu\\_DiffuMask\\_Synthesizing\\_Images\\_with\\_Pixel-level\\_Annotations\\_for\\_Semantic\\_Segmentation\\_Using\\_ICCV\\_2023\\_paper.html](https://openaccess.thecvf.com/content/ICCV2023/html/Wu_DiffuMask_Synthesizing_Images_with_Pixel-level_Annotations_for_Semantic_Segmentation_Using_ICCV_2023_paper.html)
- [4] A. C. Li, M. Prabhudesai, S. Duggal, E. Brown, and D. Pathak, “Your diffusion model is secretly a zero-shot classifier,” in *2023 IEEE/CVF International Conference on Computer Vision (ICCV)*. IEEE, pp. 2206–2217. [Online]. Available: <https://ieeexplore.ieee.org/document/10376944/>
- [5] K. Clark and P. Jaini, “Text-to-image diffusion models are zero shot classifiers,” in *Thirty-seventh Conference on Neural Information Processing Systems*. [Online]. Available: <https://openreview.net/forum?id=fxNQJVMwK2>
- [6] S. Chen, P. Sun, Y. Song, and P. Luo, “Diffusiondet: Diffusion model for object detection,” in *Proceedings of the IEEE/CVF international conference on computer vision*, 2023, pp. 19 830–19 843.
- [7] L. Karazija, I. Laina, A. Vedaldi, and C. Rupprecht, “Diffusion models for open-vocabulary segmentation,” in *European Conference on Computer Vision*. Springer, 2025, pp. 299–317.
- [8] J. Xu, S. Liu, A. Vahdat, W. Byeon, X. Wang, and S. De Mello, “Open-vocabulary panoptic segmentation with text-to-image diffusion models,” in *2023 IEEE/CVF Conference on Computer Vision and Pattern Recognition (CVPR)*. IEEE, pp. 2955–2966. [Online]. Available: <https://ieeexplore.ieee.org/document/10203350/>
- [9] A. Hertz, R. Mokady, J. Tenenbaum, K. Aberman, Y. Pritch, and D. Cohen-or, “Prompt-to-prompt image editing with cross-attention control,” in *The Eleventh International Conference on Learning Representations*. [Online]. Available: <https://openreview.net/forum?id=CDixzkzeyb>

[10] M. Cao, X. Wang, Z. Qi, Y. Shan, X. Qie, and Y. Zheng, “Masactrl: Tuning-free mutual self-attention control for consistent image synthesis and editing,” in *Proceedings of the IEEE/CVF International Conference on Computer Vision (ICCV)*, October 2023, pp. 22560–22570.

[11] H. Orgad, B. Kawar, and Y. Belinkov, “Editing implicit assumptions in text-to-image diffusion models,” in *Proceedings of the IEEE/CVF International Conference on Computer Vision*, 2023, pp. 7053–7061.

[12] J. Wang, X. Li, J. Zhang, Q. Xu, Q. Zhou, Q. Yu, L. Sheng, and D. Xu, “Diffusion model is secretly a training-free open vocabulary semantic segmenter,” *IEEE Transactions on Image Processing*, vol. 34, pp. 1895–1907, 2025.

[13] R. Tang, L. Liu, A. Pandey, Z. Jiang, G. Yang, K. Kumar, P. Stenetorp, J. Lin, and F. Ture, “What the DAAM: Interpreting stable diffusion using cross attention,” in *Proceedings of the 61st Annual Meeting of the Association for Computational Linguistics (Volume 1: Long Papers)*, A. Rogers, J. Boyd-Graber, and N. Okazaki, Eds. Association for Computational Linguistics, pp. 5644–5659. [Online]. Available: <https://aclanthology.org/2023.acl-long.310>

[14] H. Li, T. Hui, Z. Ding, J. Zhang, B. Ma, X. Wei, J. Han, and S. Liu, “Dynamic prompting of frozen text-to-image diffusion models for panoptic narrative grounding,” in *Proceedings of the 32nd ACM International Conference on Multimedia*, 2024, pp. 9485–9494.

[15] N. Tumanyan, M. Geyer, S. Bagon, and T. Dekel, “Plug-and-play diffusion features for text-driven image-to-image translation,” in *2023 IEEE/CVF Conference on Computer Vision and Pattern Recognition (CVPR)*. IEEE, pp. 1921–1930. [Online]. Available: <https://ieeexplore.ieee.org/document/10204217/>

[16] H. Chefer, Y. Alaluf, Y. Vinker, L. Wolf, and D. Cohen-Or, “Attend-and-excite: Attention-based semantic guidance for text-to-image diffusion models,” *ACM Transactions on Graphics (TOG)*, vol. 42, no. 4, pp. 1–10, 2023.

[17] W. Feng, X. He, T.-J. Fu, V. Jampani, A. R. Akula, P. Narayana, S. Basu, X. E. Wang, and W. Y. Wang, “Training-free structured diffusion guidance for compositional text-to-image synthesis,” in *The Eleventh International Conference on Learning Representations*, 2023.

[18] R. Rassin, E. Hirsch, D. Glickman, S. Ravfogel, Y. Goldberg, and G. Chechik, “Linguistic binding in diffusion models: enhancing attribute correspondence through attention map alignment,” in *Proceedings of the 37th International Conference on Neural Information Processing Systems*, 2023, pp. 3536–3559.

[19] C. Schuhmann, R. Kaczmarczyk, A. Komatsuzaki, A. Katta, R. Vencu, R. Beaumont, J. Jitsev, T. Coombes, and C. Mullis, “Laion-400m: Open dataset of clip-filtered 400 million image-text pairs,” in *NeurIPS Workshop Datacentric AI*, no. FZJ-2022-00923. Jülich Supercomputing Center, 2021.

[20] W. J. Reed, “The pareto, zipf and other power laws,” *Economics letters*, vol. 74, no. 1, pp. 15–19, 2001.

[21] S. Parashar, Z. Lin, T. Liu, X. Dong, Y. Li, D. Ramanan, J. Caverlee, and S. Kong, “The neglected tails in vision-language models,” in *Proceedings of the IEEE/CVF Conference on Computer Vision and Pattern Recognition*, 2024, pp. 12988–12997.

[22] X. Wen, B. Zhao, Y. Chen, J. Pang, and X. Qi, “What makes CLIP more robust to long-tailed pre-training data? A controlled study for transferable insights,” in *Advances in Neural Information Processing Systems*, vol. 37, 2024.

[23] I. Goodfellow, J. Pouget-Abadie, M. Mirza, B. Xu, D. Warde-Farley, S. Ozair, A. Courville, and Y. Bengio, “Generative adversarial networks,” *Communications of the ACM*, vol. 63, no. 11, pp. 139–144, 2020.

[24] J. Ho, A. Jain, and P. Abbeel, “Denoising diffusion probabilistic models,” in *Advances in Neural Information Processing Systems*, vol. 33. Curran Associates, Inc., pp. 6840–6851. [Online]. Available: <https://proceedings.neurips.cc/paper/2020/hash/4c5bcfec8584af0d967f1ab10179ca4b-Abstract.html>

[25] J. Song, C. Meng, and S. Ermon, “Denoising diffusion implicit models,” in *International Conference on Learning Representations*.

[26] R. Rombach, A. Blattmann, D. Lorenz, P. Esser, and B. Ommer, “High-resolution image synthesis with latent diffusion models,” in *2022 IEEE/CVF Conference on Computer Vision and Pattern Recognition (CVPR)*. IEEE, pp. 10674–10685. [Online]. Available: <https://ieeexplore.ieee.org/document/9878449/>

[27] J. Ho and T. Salimans, “Classifier-free diffusion guidance,” in *NeurIPS 2021 Workshop on Deep Generative Models and Downstream Applications*, 2021.

[28] L. Zhang, A. Rao, and M. Agrawala, “Adding conditional control to text-to-image diffusion models,” in *Proceedings of the IEEE/CVF International Conference on Computer Vision*, 2023, pp. 3836–3847.

[29] G. Papamakarios, E. Nalisnick, D. J. Rezende, S. Mohamed, and B. Lakshminarayanan, “Normalizing flows for probabilistic modeling and inference,” *Journal of Machine Learning Research*, vol. 22, no. 57, pp. 1–64, 2021.

[30] Y. Lipman, R. T. Chen, H. Ben-Hamu, M. Nickel, and M. Le, “Flow matching for generative modeling,” in *The Eleventh International Conference on Learning Representations*, 2022.

[31] W. Peebles and S. Xie, “Scalable diffusion models with transformers,” in *2023 IEEE/CVF International Conference on Computer Vision (ICCV)*. IEEE, pp. 4172–4182. [Online]. Available: <https://ieeexplore.ieee.org/document/10377858/>

[32] P. Marcos-Manchón, R. Alcover-Cousó, J. C. SanMiguel, and J. M. Martínez, “Open-vocabulary attention maps with token optimization for semantic segmentation in diffusion models,” in *Proceedings of the IEEE/CVF Conference on Computer Vision and Pattern Recognition*, 2024, pp. 9242–9252.

[33] J. Tian, L. Aggarwal, A. Colaco, Z. Kira, and M. Gonzalez-Franco, “Diffuse attend and segment: Unsupervised zero-shot segmentation using stable diffusion,” in *Proceedings of the IEEE/CVF Conference on Computer Vision and Pattern Recognition*, pp. 3554–3563. [Online]. Available: [https://openaccess.thecvf.com/content/CVPR2024/html/Tian\\_Diffuse\\_Attend\\_and\\_Segment\\_Uncervised\\_Zero-Shot\\_Segmentation\\_using\\_Stable\\_Diffusion\\_CVPR\\_2024\\_paper.html](https://openaccess.thecvf.com/content/CVPR2024/html/Tian_Diffuse_Attend_and_Segment_Uncervised_Zero-Shot_Segmentation_using_Stable_Diffusion_CVPR_2024_paper.html)

[34] D. Yang, R. Dong, J. Ji, Y. Ma, H. Wang, X. Sun, and R. Ji, “Exploring phrase-level grounding with text-to-image diffusion model,” in *European Conference on Computer Vision*. Springer, 2024.

[35] A. Kirillov, E. Mintun, N. Ravi, H. Mao, C. Rolland, L. Gustafson, T. Xiao, S. Whitehead, A. C. Berg, W.-Y. Lo, P. Dollár, and R. Girshick, “Segment anything,” in *2023 IEEE/CVF International Conference on Computer Vision (ICCV)*. IEEE, pp. 3992–4003. [Online]. Available: <https://ieeexplore.ieee.org/document/10378323/>

[36] D. H. Park, G. Luo, C. Toste, S. Azadi, X. Liu, M. Karalashvili, A. Rohrbach, and T. Darrell, “Shape-guided diffusion with inside-outside attention,” in *Proceedings of the IEEE/CVF Winter Conference on Applications of Computer Vision*, 2024, pp. 4198–4207.

[37] H. Nam, G. Kwon, G. Y. Park, and J. C. Ye, “Contrastive denoising score for text-guided latent diffusion image editing,” in *2024 IEEE/CVF Conference on Computer Vision and Pattern Recognition (CVPR)*. IEEE, pp. 9192–9201. [Online]. Available: <https://ieeexplore.ieee.org/document/10657048/>

[38] S. Hong, G. Lee, W. Jang, and S. Kim, “Improving sample quality of diffusion models using self-attention guidance,” in *Proceedings of the IEEE/CVF International Conference on Computer Vision*, 2023, pp. 7462–7471.

[39] A. Vaswani, N. Shazeer, N. Parmar, J. Uszkoreit, L. Jones, A. N. Gomez, L. U. Kaiser, and I. Polosukhin, “Attention is all you need,” in *Advances in Neural Information Processing Systems*, I. Guyon, U. V. Luxburg, S. Bengio, H. Wallach, R. Fergus, S. Vishwanathan, and R. Garnett, Eds., vol. 30. Curran Associates, Inc., 2017. [Online]. Available: [https://proceedings.neurips.cc/paper\\_files/paper/2017/file/3f5ee243547dee91fb0d053c1c4a845aa-Paper.pdf](https://proceedings.neurips.cc/paper_files/paper/2017/file/3f5ee243547dee91fb0d053c1c4a845aa-Paper.pdf)

[40] D. Podell, Z. English, K. Lacey, A. Blattmann, T. Dockhorn, J. Müller, J. Penna, and R. Rombach, “Sdxl: Improving latent diffusion models for high-resolution image synthesis,” in *The Twelfth International Conference on Learning Representations*, 2023.

[41] J. Chen, Y. Jincheng, G. Chongjian, L. Yao, E. Xie, Z. Wang, J. Kwok, P. Luo, H. Lu, and Z. Li, “Pixart- $\alpha$ : Fast training of diffusion transformer for photorealistic text-to-image synthesis,” in *The Twelfth International Conference on Learning Representations*, 2023.

[42] P. Esser, S. Kulal, A. Blattmann, R. Entezari, J. Müller, H. Saini, Y. Levi, D. Lorenz, A. Sauer, F. Boesel *et al.*, “Scaling rectified flow transformers for high-resolution image synthesis,” in *Forty-first International Conference on Machine Learning*, 2024.

[43] L. Xu, M. Bennamoun, F. Boussaid, H. Laga, W. Ouyang, and D. Xu, “Mctformer+: Multi-class token transformer for weakly supervised semantic segmentation,” *IEEE Transactions on Pattern Analysis and Machine Intelligence*, 2024.

[44] D. Kingma, T. Salimans, B. Poole, and J. Ho, “Variational diffusion models,” *Advances in neural information processing systems*, vol. 34, pp. 21696–21707, 2021.

[45] Y. Song, C. Durkan, I. Murray, and S. Ermon, “Maximum likelihood training of score-based diffusion models,” *Advances in neural information processing systems*, vol. 34, pp. 1415–1428, 2021.

[46] Y. Song, J. Sohl-Dickstein, D. P. Kingma, A. Kumar, S. Ermon, and B. Poole, “Score-based generative modeling through stochastic differential equations,” in *International Conference on Learning Representations*.

- [47] D. Kingma and R. Gao, "Understanding diffusion objectives as the elbo with simple data augmentation," *Advances in Neural Information Processing Systems*, vol. 36, 2024.
- [48] J. Sohl-Dickstein, E. Weiss, N. Maheswaranathan, and S. Ganguli, "Deep unsupervised learning using nonequilibrium thermodynamics," in *Proceedings of the 32nd International Conference on Machine Learning*. PMLR, pp. 2256–2265, ISSN: 1938-7228. [Online]. Available: <https://proceedings.mlr.press/v37/sohl-dickstein15.html>
- [49] T. Salimans and J. Ho, "Progressive distillation for fast sampling of diffusion models," in *International Conference on Learning Representations*.
- [50] M. Everingham, L. Van Gool, C. K. Williams, J. Winn, and A. Zisserman, "The pascal visual object classes (voc) challenge," *International journal of computer vision*, vol. 88, pp. 303–338, 2010.
- [51] R. Mottaghi, X. Chen, X. Liu, N.-G. Cho, S.-W. Lee, S. Fidler, R. Urtasun, and A. Yuille, "The role of context for object detection and semantic segmentation in the wild," in *Proceedings of the IEEE conference on computer vision and pattern recognition*, 2014, pp. 891–898.
- [52] T.-Y. Lin, M. Maire, S. Belongie, J. Hays, P. Perona, D. Ramanan, P. Dollár, and C. L. Zitnick, "Microsoft coco: Common objects in context," in *Computer Vision-ECCV 2014: 13th European Conference, Zurich, Switzerland, September 6-12, 2014, Proceedings, Part V 13*. Springer, 2014, pp. 740–755.
- [53] B. Zhou, H. Zhao, X. Puig, T. Xiao, S. Fidler, A. Barriuso, and A. Torralba, "Semantic understanding of scenes through the ade20k dataset," *International Journal of Computer Vision*, vol. 127, pp. 302–321, 2019.
- [54] B. F. Labs, "Flux," <https://github.com/black-forest-labs/flux>, 2024.
- [55] T. Ren, S. Liu, A. Zeng, J. Lin, K. Li, H. Cao, J. Chen, X. Huang, Y. Chen, F. Yan, Z. Zeng, H. Zhang, F. Li, J. Yang, H. Li, Q. Jiang, and L. Zhang, "Grounded sam: Assembling open-world models for diverse visual tasks," 2024.
- [56] Damian0815, "Compel: A prompting enhancement library for transformers-type text embedding systems." <https://github.com/damian0815/compel>, 2025, accessed: 2025-05-23.
- [57] T. Wolf, L. Debut, V. Sanh, J. Chaumond, C. Delangue, A. Moi, P. Cistac, T. Rault, R. Louf, M. Funtowicz, J. Davison, S. Shleifer, P. von Platen, C. Ma, Y. Jernite, J. Plu, C. Xu, T. L. Scao, S. Gugger, M. Drame, Q. Lhoest, and A. M. Rush, "Transformers: State-of-the-art natural language processing," in *Proceedings of the 2020 Conference on Empirical Methods in Natural Language Processing: System Demonstrations*. Online: Association for Computational Linguistics, Oct. 2020, pp. 38–45. [Online]. Available: <https://www.aclweb.org/anthology/2020.emnlp-demos.6>
- [58] P. von Platen, S. Patil, A. Lozhkov, P. Cuénca, N. Lambert, K. Rasul, M. Davaadorj, D. Nair, S. Paul, W. Berman, Y. Xu, S. Liu, and T. Wolf, "Diffusers: State-of-the-art diffusion models," <https://github.com/huggingface/diffusers>, 2022.